CRANFIELD UNIVERSITY

MSc Autonomous Vehicles Dynamics and Control

Sensor Fusion: Architectures, Algorithms and Applications

Assignment - Civil GPS Jammer Geolocation from UAV using Received Signal Strength

Author: **Álvaro Fernández Cobo**
Student Number: **253316**

January 27, 2017
Academic Year: 2016/2017

This page intentionally left blank.

Contents

Contents **3**

List of Figures **5**

1 Introduction **7**

2 Problem Formulation **8**

2.1 Geolocation Concept 8

2.2 General Filter Equations 9

2.3 UAV Navigation and Control 10

3 Isotropic Radiation pattern GPS Jammer Geolocation **11**

3.1 Extended Kalman Filter 11

3.2 Unscented Kalman Filter 12

3.3 Particle Filter 15

3.4 Performance Analysis 18

4 GPS Jammer Geolocation under Anisotropic Radiation pattern **21**

4.1 Original Filters Performance 21

4.2 EKF with smoothing 24

4.3 Augmented UKF and EKF 24

4.3.1 EKF with changing reference step 25

4.4 Alternative Filters Performance 26

5 Conclusions **29**

References **31**

This page intentionally left blank.

List of Figures

1 Search Scenario 7
2 EKF estimation example 13
3 UKF estimation example 15
4 PF estimation example 17
5 RMSE evolution. Isotropic case 19
6 Final Estimation Error Distribution. Isotropic case 20
7 Mean Filter Execution Time. Isotropic case 20
8 Transmitter Gain with respect to Azimuth and Elevation 21
9 EKF performance example under anisotropic conditions 22
10 RMSE evolution. Anisotropic case. Original filters 22
11 Final Estimation Error Distribution. Anisotropic case. Original Filters 23
12 Mean Filter Execution Time. Anisotropic case. Original filters 23
13 Example of Transmitter gain estimation with augmented EKF 26
14 RMSE evolution. Anisotropic case. Alternative Filters 27
15 Final Estimation Error Distribution. Anisotropic case. Alternative Filters 27
16 Mean Filter Execution Time. Anisotropic case. Alternative Filters . . . 28

This page intentionally left blank.

1 Introduction

The aim of this assignment is to investigate civil GPS Jammer geolocation. In particular, several filtering solutions have been developed and are analysed throughout this document. The filter is to be run on board a UAV fitted with a Received Signal Strength Indicator (RSSI), which measures the power of the received radio signal. The developed filter has to be able to geolocate the Civil GPS Jammer based on those measurements.

This document presents the most significant results achieved during the development of the filter, which were obtained by means of simulations conducted on MATLAB. The proposed search area is a 12-by-12 km square in which the GPS Jammer and UAV are initially randomly placed (see Figure 1). The Jammer is assumed to be on the ground and static. Two different scenarios are considered:

- **Isotropic Case**: In the ideal case, the GPS Jammer has a perfectly isotropic radiation pattern.
- **Anisotropic Case**: The isotropic assumption is relieved. This is because the target, namely a vehicle harbouring the GPS Jammer, would have a great impact in the radiation pattern outside the car. The energy will primarily escape through the windscreen and windows.

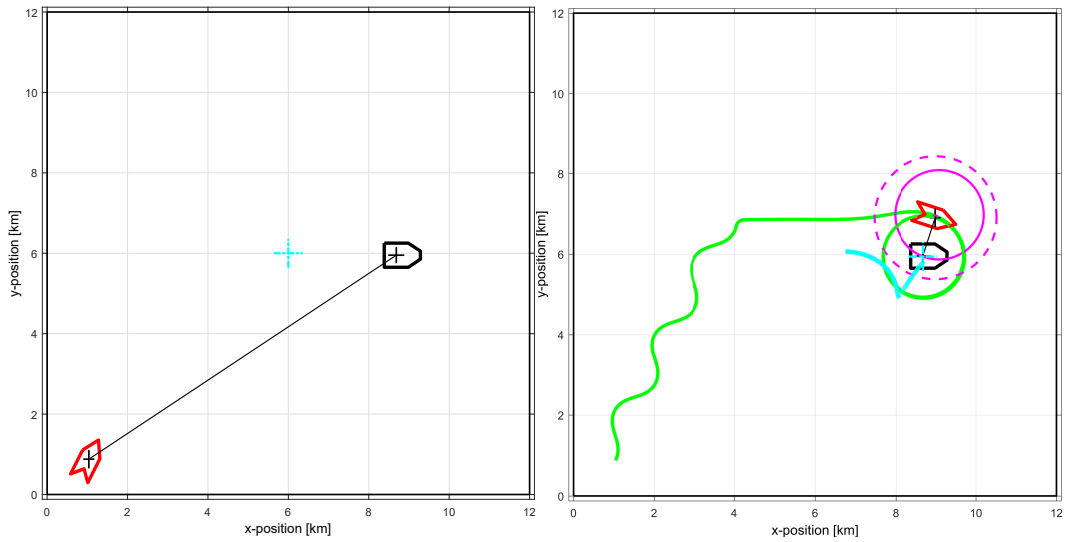

(a) Beginning of the Search (b) End of the Search

Figure 1: Search Scenario

Three different filtering algorithms are mainly analysed: Extended Kalman Filter (EKF), Unscented Kalman Filter (UKF) and Particle Filter (PF). The performance of all this three filters in the isotropic case is analysed in Section 3.

Later, the same algorithms are tested under the anisotropic GPS Jammer radiation pattern and the obtained results are presented and discussed in Section 4. Furthermore, different modifications are proposed in Section 4 in order to improve the performance of the original algorithms.

The code employed within this assignment is available in the next link `https://github.com/2afc93/jammer_location_prj`

2 Problem Formulation

This section is devoted to describe the proposed problem from a analytical point of view. The final equations employed in the simulations are derived in the first part.

Later on the second part, the general equations for the filters are presented.

2.1 Geolocation Concept

The geolocation strategy employed is primarily based on Friis' equation of transmission (1)

$$P_r = P_t G_t G_r \left(\frac{\lambda}{4\pi r}\right)^2 \tag{1}$$

where P_r, P_t, G_r, G_t are the received/transmitted power and the receiver/transmitter gains respectively. λ is the wavelength, particularly, that at the L1 frequency[1], $\lambda \approx 20$ cm, and r is the slant range or line-of-sight distance between the UAV and the target.

The transmitted power P_t is assumed to be constant for a given GPS Jammer. Nevertheless, the emitted powers vary greatly between different retail Jammer models, from miliwatts to more than half a Watt. As a result, it is not viable to estimate range from received power P_r.

However, the geolocation technique can be developed employing received power ratios because the transmitter power is cancelled, as can be deduced from Friis' equation (1). Thus, the power ratio between two instants is related to the slant range ratio, as specified in equation (2)

$$\frac{P_{r,2}}{P_{r,1}} = \frac{G_{t,2}}{G_{t,1}} \left(\frac{r_1}{r_2}\right)^2 \tag{2}$$

where the subscript numbers 1, 2 mean two different iterations. The power measurements $P_{r,i}$ received by the antenna on board the UAV will be noisy. The noise power

[1]Frequency band employed as carrier of civilian-use GPS modulated signals. GPS Jammers emit mainly around this frequency

has been assessed by considering thermal noise according to Johnson-Nyquist equation (3)

$$P_{th} = k_b T B F \tag{3}$$

where P_{th}, T, B, F are, respectively the thermal noise power, the absolute temperature the sensor sees, the jammer bandwidth and a model factor ($\approx 1 - 2$ dB) and k_b is the Boltzman constant.

As it was mentioned before, the search area is a 12 km $\times$ 12 km square. The jammer is randomly placed somewhere within a 4 km $\times$ 4 km square in the centre of the search area. The UAV will start searching with a random heading from the South-West corner.

The range $\underline{r}$ is defined, according to equation (4), as the relative position between the jammer and the UAV

$$\underline{r} = \underline{x}_t - \underline{x}_s \tag{4}$$

where $\underline{x}_t$, $\underline{x}_s$ are, relatively, the position of the jammer and UAV, with coordinates

$$\underline{x}_t = \begin{bmatrix} x_t \\ y_t \\ 0 \end{bmatrix}, \underline{x}_s = \begin{bmatrix} x_s \\ y_s \\ h_0 \end{bmatrix}$$

The slant range r is the module of $\underline{r}$ given by equation (5)

$$r = \sqrt{(x_t - x_s)^2 + (y_t - y_s)^2 + h_0^2} \tag{5}$$

Equations (2) and (5) can be combined into a single expression relating power ratios, jammer-UAV relative position. Such a expression is shown in equation (6)

$$\alpha_{k,i} = \frac{P_{r,k}}{P_{r,i}} = \frac{G_{t,k}}{G_{t,i}} \frac{(x_t - x_{s,i})^2 + (y_t - y_{s,i})^2 + h_0^2}{(x_t - x_{s,k})^2 + (y_t - y_{s,k})^2 + h_0^2} \tag{6}$$

where $\alpha_{k,i}$ is defined as the received power ratio at step k with respect to step i.

2.2 General Filter Equations

Firstly, the dynamics of the target have to be modelled. As the jammer remains stationary at a given position, the dynamic model is that of a static system according to equation (7)

$$\begin{bmatrix} x_t \\ y_t \end{bmatrix}_k = \underbrace{\begin{bmatrix} 1 & 0 \\ 0 & 1 \end{bmatrix}}_{F} \begin{bmatrix} x_t \\ y_t \end{bmatrix}_{k-1} + v_k \tag{7}$$

where F is the process matrix and v_k is additive Gaussian noise. v_k is employed to take into account the effect of unmodeled dynamics, which is not necessary in this case as

jammer is assumed to remain perfectly motionless. However, in practise, the inclusion of v_k helps the filter to converge more rapidly. Thus, we have the process noise matrix Q defined by equation (8).

$$Q = \begin{bmatrix} \sigma_{v_x}^2 & 0 \\ 0 & \sigma_{v_y}^2 \end{bmatrix} \tag{8}$$

For now on, the predicted horizontal position of the jammer at step k will be given by

$$\underline{x}_k = \begin{bmatrix} x_k \\ y_k \end{bmatrix}$$

Secondly, the measurement equation need to be defined according to the non-linear relation shown in equation (9)

$$\underline{z}_k = h(\underline{x}_k) + w_k \tag{9}$$

where w_k is the additive Gaussian noise of the measurement.

Particularly, $\underline{z}_k$ will be rename as $\underline{z}_{k,i}$ and is an scalar representing the received power ratios between steps k and i. Similarly, the measurement function $h(\underline{x}_k)$ will be rename as $h_{k,i}(\underline{x}_k)$ and is equal to $\alpha_{i,k}$, which was defined in equation (6) as a function of the jammer position $\underline{x}_t$ (now $\underline{x}_k$), the UAV positions $\underline{x}_{s,i}$ and $\underline{x}_{s,k}$ and the transmitter gains ratio $G_{t,k}/G_{t,i}$.

In order to implement the EKF, the first-order partial derivatives or Jacobian matrix is needed. Such matrix $H_{k,i}(\underline{x}_k)$ is defined by equation (10) as a function of the jammer position $\underline{x}_t$ (now $\underline{x}_k$), the UAV positions $\underline{x}_{s,i}$ and $\underline{x}_{s,k}$ and the transmitter gains ratio $G_{t,k}/G_{t,i}$.

$$H_{k,i}^T(\underline{x}_k) = 2\frac{G_{t,k}}{G_{t,i}} \begin{bmatrix} \frac{x_k - x_{s,i}}{\left(x_k - x_{s,k}\right)^2 + \left(y_k - y_{s,k}\right)^2 + {h_0}^2} - \frac{\left((x_k - x_{s,i})^2 + (y_k - y_{s,i})^2 + {h_0}^2\right)\left(x_k - x_{s,k}\right)}{\left(\left(x_k - x_{s,k}\right)^2 + \left(y_k - y_{s,k}\right)^2 + {h_0}^2\right)^2} \\ \\ \frac{y_k - y_{s,i}}{\left(x_k - x_{s,k}\right)^2 + \left(y_k - y_{s,k}\right)^2 + {h_0}^2} - \frac{\left((x_k - x_{s,i})^2 + (y_k - y_{s,i})^2 + {h_0}^2\right)\left(y_k - y_{s,k}\right)}{\left(\left(x_k - x_{s,k}\right)^2 + \left(y_k - y_{s,k}\right)^2 + {h_0}^2\right)^2} \end{bmatrix} \tag{10}$$

In general, the first step of the simulation will be used as a reference to calculate the received power and range ratios, so $i = 1$.

2.3 UAV Navigation and Control

The Navigation and Guidance problems are out of the scope of this assignment. Firstly, the UAV is assumed to precisely know its position and orientation with respect to the world reference system at every moment.

Secondly, UAV altitude and speed are kept constant during the entire mission, $h_0 = 125$ m and $V_g = 28.3$ m/s [2]. The UAV guidance strategy consists of two phases:

1. **Flyby**: A winding or weaving path with the given orientation is firstly followed in order to get rid of the so-called "ghost jammer". Moreover, thanks to this strategy, the observability is increased and it also gives time to the estimator to converge.

2. **Orbital Adaptation**: Once the flyby phase is completed, the UAV heads to the target location. As velocity and altitude are kept constant, the estimated jammer position is employed to generate heading commands. The proposed guidance scheme is called Lyapunov Vector Field Guidance (LVFG) [1].

Both Flyby and Orbital Adaptation guidance strategies were already implemented in the provided code.

3 Isotropic Radiation pattern GPS Jammer Geolocation

The Isotropic Radiation pattern assumption implies that the received power does not depend on the UAV position. Or, which is the same thing, the transmitter gain ratio $G_{t,k}/G_{t,i}$ is equal to unity and, hence, can be removed from the expression of $\alpha_{k,i}$. As stated in Section 1, three different filtering strategies are to be designed: EKF, UKF and PF.

This section is devoted to present the resultant filters and analyse their performance in the ideal case.

3.1 Extended Kalman Filter

The EKF is a widely known and employed sub-optimal estimator that broadens the capabilities of the Linear Kalman Filter (LKF) to those applications in which either the process or the measurement cannot be expressed as a linear relationship between the state variables and the output.

The EKF is a nonlinear version of the LKF in which the linearisation is made about the filter's mean state estimate. It has been widely studied. Nowadays, there are multiple modified and improved versions of the original one.

[2] Whereas the given assignment document states that $V_g = 30$ m/s and $h_0 = 200$ m, the values in the provided code were different and the ones that were finally employed.

An exhaustive derivation of the equations is not made within this document. Such derivation can be found in numberless books and papers. However, the final coded equations are presented below together with the values employed for the different parameters.

The jammer state propagation is done according to equation, which is (7)

$$\underline{\hat{x}}_{k|k-1} = F\underline{\hat{x}}_{k-1|k-1} \tag{11}$$

The covariance matrix is also propagated according to equation (12)

$$P_{k|k-1} = FP_{k-1|k-1}F^T + \Gamma Q\Gamma^T \tag{12}$$

where $\Gamma = [1]$ and

$$Q = \begin{bmatrix} 0.1 & 0 \\ 0 & 0.1 \end{bmatrix}$$

The non-linear measurement is given by the expression of $\alpha_{k,i}$ in equation (6). The estimated measurement is $h_k = \alpha_{k,1}(\underline{\hat{x}}_{k|k-1})$. Taking into account the measurement at step k, we calculate the difference $v_k = z_k - h_k$.

To compute the Kalman Gain it is necessary to previously calculate the innovation matrix given by equation 13

$$S = H_k P_{k|k-1} H^T + R \tag{13}$$

where H_k is the Jacobian matrix in equation (10) evaluated at $\underline{x}_{k|k-1}$ and R is the measurement covariance noise matrix. Particularly, $R = [0.1^2]$ has been employed. Then, the Kalman gain matrix is given by

$$K_k = P_{k|k-1}H_k^T S^{-1}$$

Finally, the updated state vector and covariance matrix are given by equations (14) (15).

$$\underline{\hat{x}}_{k|k} = \underline{\hat{x}}_{k|k-1} + K_k v_k \tag{14}$$

$$P_{k|k} = P_{k|k-1} - K_k H_k P_{k|k-1} \tag{15}$$

The function provided during the laboratories of *Sensor Fusion: Algorithms, Architectures and Applications* module was employed as a template where the above exposed equations were injected.

3.2 Unscented Kalman Filter

Similarly to EKF, UKF is a modification of the LKF in order to enable its application to system with non-linear dynamics or measurements. It was first introduced by 1997 by S.J. Julier and J.K. Uhlmann.

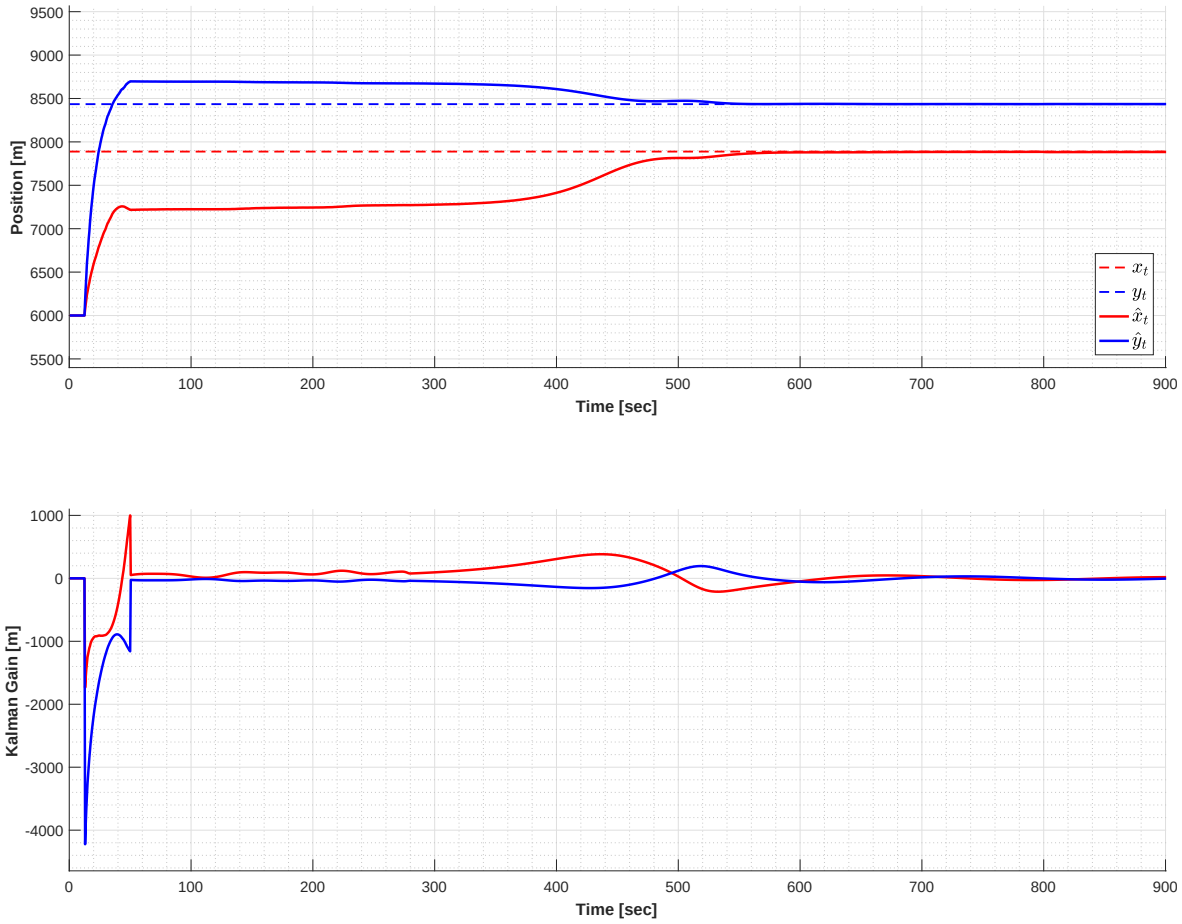

Figure 2: EKF estimation example

The algorithm is based in the Unscented Transformation, which computes the new state $\underline{\hat{x}}_k$ and covariance P_k from using a set of so-called *sigma points* around the former state estimation. An exhaustive derivation of the algorithm and its foundations can be found in [2]. Only the final equations are presented below.

As the dynamic of the system is linear, the prediction step is done in the same way as in EKF, employing equations (11), (12).

Having $\underline{x}_{k|k-1}$ and $P_{k|k-1}$, a set of $2n+1$ *sigma points* and weights is defined as shown in equation (16). n is the dimension of the state vector.

$$\begin{aligned} \mathcal{X}_0 &= x_{k|k-1} & W_0 &= \lambda/(n+\lambda) \\ \mathcal{X}_i &= x_{k|k-1} + \left(\sqrt{(n+\lambda)P_{k|k-1}}\right)_i & W_i &= 1/2(n+\lambda) \\ \mathcal{X}_{i+n} &= x_{k|k-1} - \left(\sqrt{(n+\lambda)P_{k|k-1}}\right)_i & W_{i+n} &= 1/2(n+\lambda) \end{aligned} \tag{16}$$

$$\lambda = \alpha^2(n+\kappa) - n \tag{17}$$

The position of the *sigma points* determine the performance of the filter. Hence, it is important to carefully choose the values of the different parameters affecting their position. In this particular case, $\kappa = 2$ and $\alpha = 0.4$ were the values that provide the best results.

The nonlinear measurement function in equation (6) is evaluated to get the set of transformed *sigma points*

$$\mathcal{Y}_i = h[\mathcal{X}_i]$$

Then the mean is computed according to

$$\overline{y} = \sum_{i=0}^{2n} \mathcal{Y}_i \, W_i$$

and the innovation covariance is defined as

$$P_{yy} = \sum_{i=0}^{n} \left(W_i \, \left[\mathcal{Y}_i - \bar{y}\right] \left[\mathcal{Y}_i - \bar{y}\right]^T \right) \, + R$$

.

Finally, the cross covariance matrix is calculated according to equation (18).

$$P_{xy} = \sum_{i=0}^{2n} W_i \, \left[\mathcal{X}_i - \underline{\hat{x}}_{k|k-1}\right] \left[z_k - \bar{y}\right]^T \tag{18}$$

Then, similarly to the process that is followed for the EKF, the updated state $\underline{\hat{x}}_{k|k}$, covariance matrix $P_{k|k}$ and the Kalman Gain K_k is computed according to equations (19) (20) (21) (22).

$$v_k = z_k - \bar{y}_k \tag{19}$$

$$K_k = P_{xy} P_{yy}^{-1} \tag{20}$$

$$\underline{\hat{x}}_{k|k} = \underline{\hat{x}}_{k|k-1} + K_k \, v_k \tag{21}$$

$$P_{k|k} = P_{k|k-1} - K_k \, P_{yy} K_k^T \tag{22}$$

The matrices Q and R employed in the UKF have been identical to those employed in EKF. An example of the performance of the UKF is shown in Figure 3.

The developed filter is based on that coded by Yi Cao from Cranfield University [3], which is based on the paper [4].

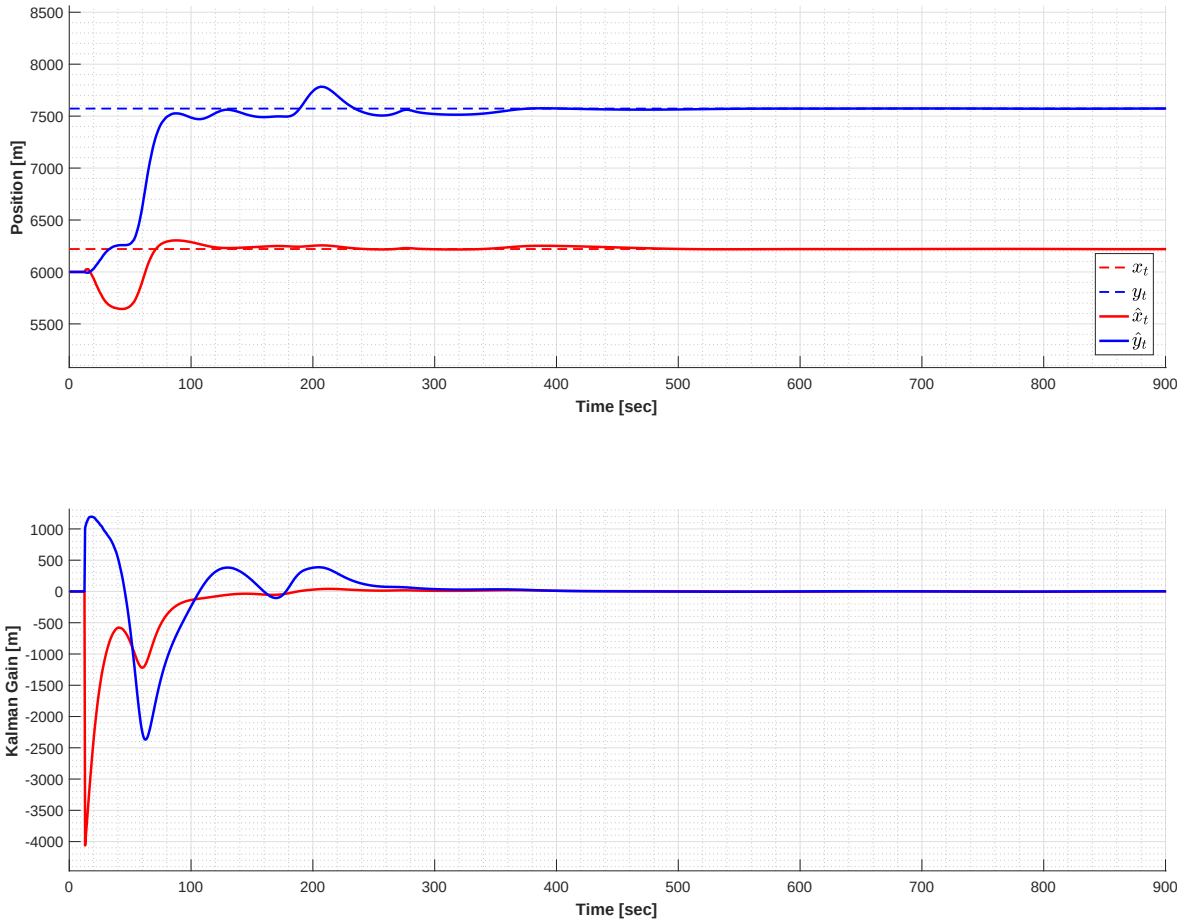

Figure 3: UKF estimation example

3.3 Particle Filter

Particles Filter or Sequential Monte Carlo methods is the third analysed approach to the filtering problem that is going to be analysed within this document.

As stated in [5], the foundation of this estimation strategy lies in computing the posterior density function and estimated state from a set of random samples with associated weights.

In the first estimation step, an initial particle sample has to be initialise. In our particular case, we get a set of N particles uniformly distributed within the 6 km x 6 km region where the jammer is to be located. As no a priori information is available, all the samples x^i from the initial set are equally probable and, thus, have the same initial $w^i = 1/N$.

Firstly, the particle population is propagated from $k-1$ to k according to

$$x_k^i = F\, x_{k-1}^i + v_k$$

where $v_k \approx N(0, sqrt(Q))$ is a 2-dimension random sample from the normal distribution with mean 0 and standard deviation σ_{v_x}, σ_{v_y}.

Secondly, the weights are updated taking into account the current measurement. In order to do this, nonlinear measurement function is evaluated at the propagated particle set, having

$$y^i = h(x_k^i)$$

The difference between the measurement and the transformed points is calculated

$$d_k^i = z_k - y^i$$

and the weights are updated according to

$$w_k^i = w_{k-1}^i \, p(d_k^i | (0, \sigma_w))$$

where $p(x|(0, \sigma_w))$ is the normal probability function with mean 0 and typical deviation σ_w evaluated at x.

Finally, the estimated state is computed as the weighted mean of the particles within the sample

$$\underline{\hat{x}}_k = \sum_{i=1}^{N} w_k^i \, x_k^i$$

.

An issue of this filtering strategy is the so-called *sample degeneracy problem*. In practise, the iteration of the particle filter leads to a population where just a few particles will have a significant weight. The resampling prevents this problem but brings another one: the *sample impoverishment*. As those particles with larger weights are more likely to be drawn during the resampling, the diversity of the population will gradually decrease.

However, resampling is required to remove those particle with lowest weights. The correct tuning of the process noise and measurement covariance matrices will help to fight against the sample impoverishment.

The employed resampling algorithm is called *systematic resampling*. The parameter that decides whether the resampling is made or not is the effective sample size defined in (23). If N_{eff} is smaller than a given value, then the resampling is made.

$$N_{eff} = \frac{1}{\sum_{i=1}^{N} (w_k^i)^2} \tag{23}$$

The values of Q and R where changed with respect to those used in EKF and UKF. The process covariance matrix was set to

$$Q = \begin{bmatrix} 10 & 0 \\ 0 & 10 \end{bmatrix}$$

and the noise covariance matrix $R = [100]$. This way, we ensure that the particles are going to *evolve* during the prediction step, avoiding the sample impoverishment. Moreover, with a higher noise covariance, we prevent the weights from going all to zero in case a highly deviated measurement arrived.

The effective sample size parameter N_{eff} that has shown the best performance has been $N_{eff} = 0.65$. Finally, three sample sizes have been tested, $N = 150$, $N = 300$ and $N = 500$.

Figure 4 depicts an example of state estimation employing the PF. The chart in the bottom is specially interesting as it shows how the particle population gradually evolve until converging to the estimation which, hopefully, would be similar to the true state.

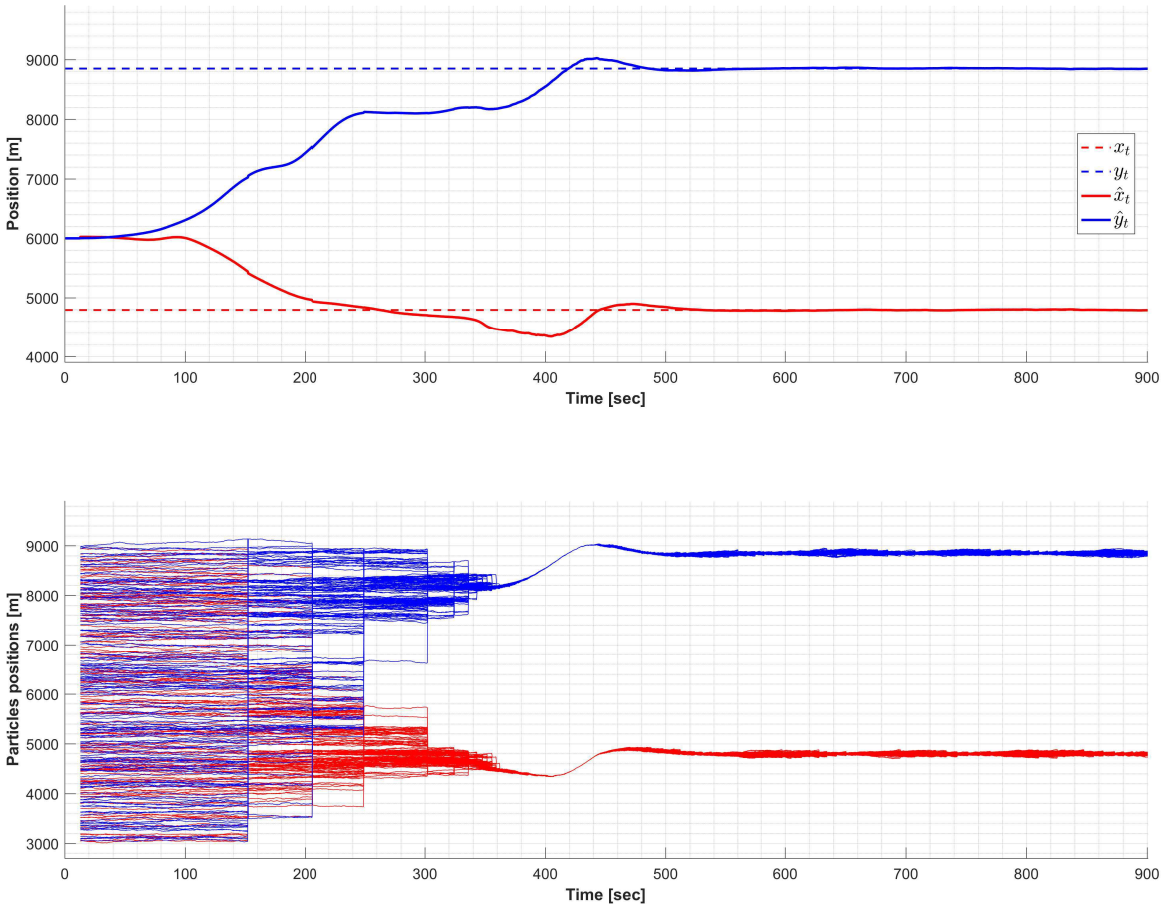

Figure 4: PF estimation example

The developed PF was adapted from the filter programmed by Diego Andrés Alvarez Marín from Universidad Nacional de Colombia [6], which is based on [5].

3.4 Performance Analysis

In order to assess their performance, all the 3 filters have been tested under the same conditions. The jammer position and transmitter power have been set as variable parameters while the initial UAV heading has remained constant and equal to 45^o.

For 11 transmitter powers ranging from 50 to 650 mW, 25 different jammer positions within the 6 km x 6 km square have been tested. In total, 275 simulations have been performed for each filter.

Moreover, 3 different population sizes have been tested in the particle filter: $N = 150, 300, 500$.

The range error has been employed as the parameter to assess the performance of the different filters. For a given realisation i, Equation (24) defines the range error at step k.

$$\epsilon_k^i = \sqrt{(x_t^i - \hat{x}_k^i)^2 + (y_t^i - \hat{y}_k^i)^2} \tag{24}$$

For a set of n realisations, the Root Mean-Square Error (RMSE) at step k is defined, according to Equation 25, as the square root of the mean of the squared range errors.

$$RMSE_k = \sqrt{\frac{1}{n}\sum_{i=1}^{n}(\epsilon_k^i)^2} \tag{25}$$

Figure 5 depicts the temporal evolution of the RMSE of the 275 simulations. It can be noticed that the RMSE of EKF almost overlap that of the UKF. Both estimators converge to the true state very quickly.

On the other hand, the three PFs have similar RMSE trends which are significantly worse than those of the EKF and the UKF.

A better perspective of the performance can be achieved by analysing Figure 6, which classifies the different realisations according to the final error.

The final error has been computed as the range error mean of the last N_f steps

$$\epsilon_f^i = \frac{1}{N_f}\sum_{k=k_f-N_f}^{k_f}\epsilon_k^i$$

where k_f is the final step and $N_f = 200$.

Figure 6 shows again that EKF and UKF clearly overtake the three PFs. An accuracy under three metres is almost guaranteed and 80% of the realisations achieved an error

under one metre. Despite the better performance of the PF with $N = 500$ with respect the two others PFs, it cannot get even closer to the performance of Kalman Filters.

Additionally, Figure 7 provides an insight into the computational cost of each of the implemented filters. It can be noticed that the Sequential Monte Carlo (SMC) methods have run times which are two order of magnitude higher than the Kalman Filters, which are executed in less than one half of a millisecond.

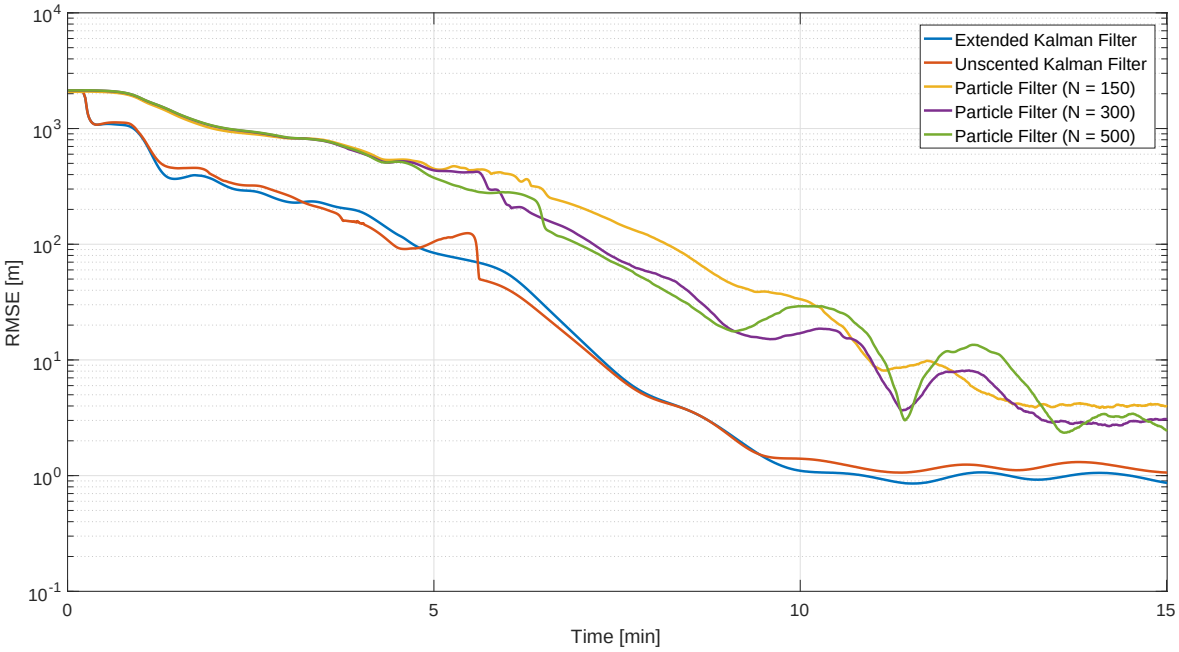

Figure 5: RMSE evolution. Isotropic case

All factors considered, there is no reason for hesitation in this particular application. Both EKF and UKF have a significantly better performance with substantially smaller execution times.

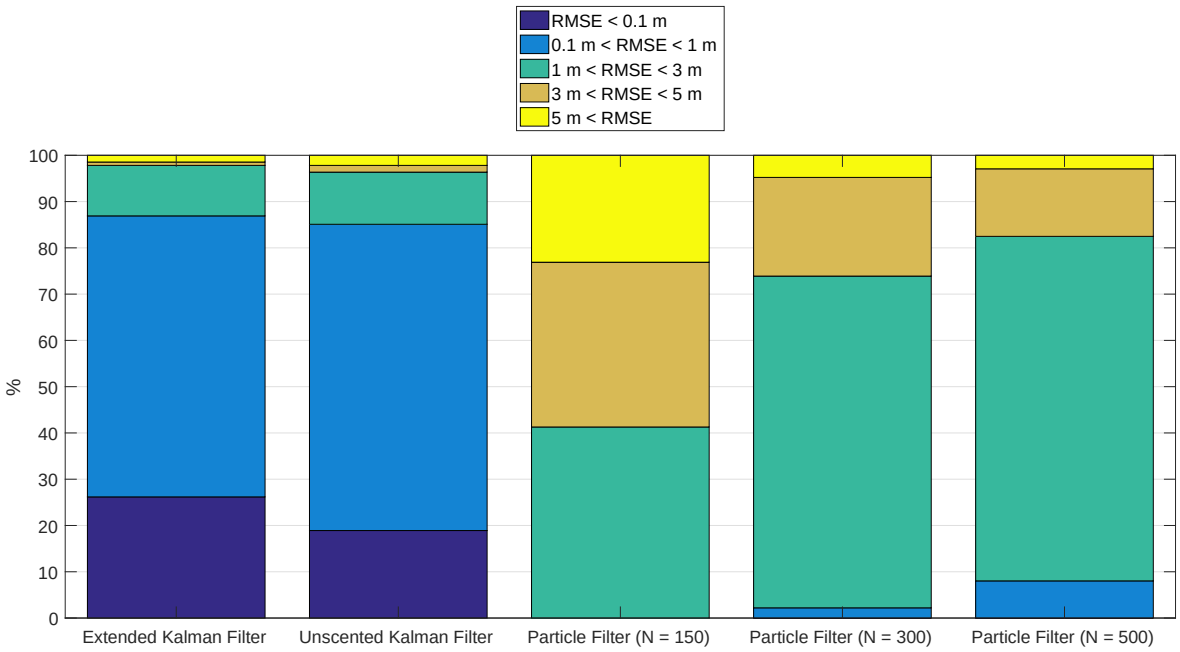

Figure 6: Final Estimation Error Distribution. Isotropic case

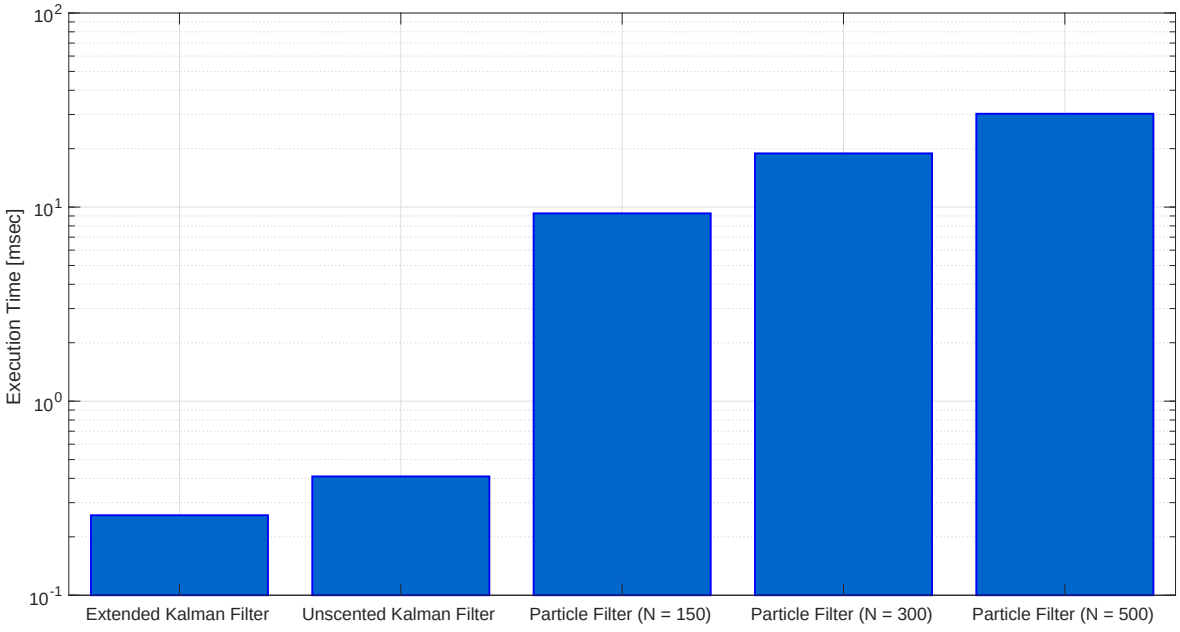

Figure 7: Mean Filter Execution Time. Isotropic case

4 GPS Jammer Geolocation under Anisotropic Radiation pattern

Within this section, a more realistic approach to the GPS Jammer location problem is adopted. The Anisotropic Radiation pattern means that the transmitter gains ratio $G_{t,k}/G_{t,i}$ is no longer unity. This is due to the fact that the way radiation propagates is affected by the vehicle harbouring the GPS jammer. Figure 8 depicts the transmitter gain map for each elevation θ and azimuth ϕ of the UAV with respect to the jammer. However, this gain map is not known a priori.

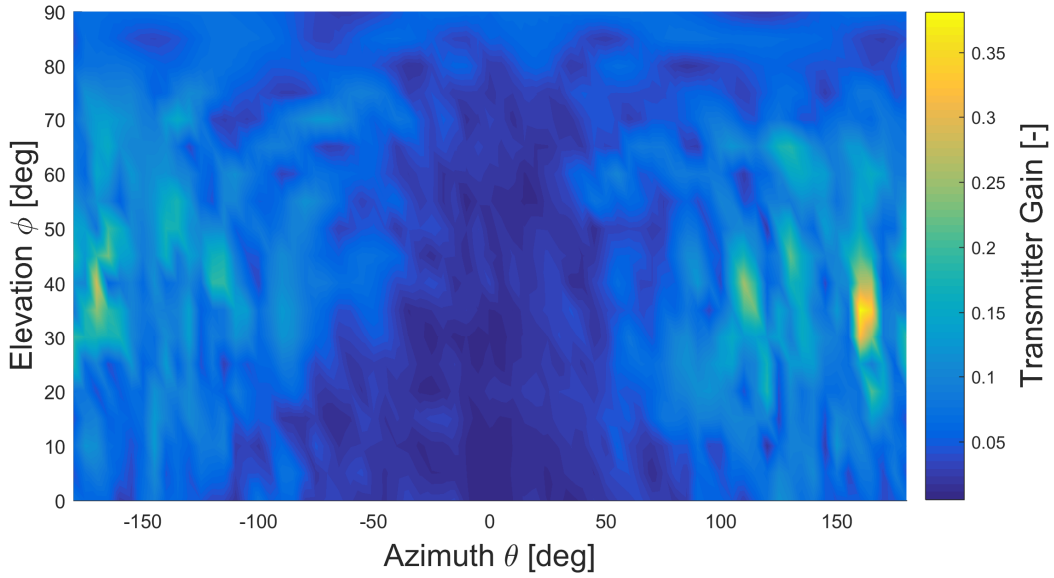

Figure 8: Transmitter Gain with respect to Azimuth and Elevation

4.1 Original Filters Performance

The performance of the filters presented in Section 3 is first analysed under the anisotropic radiation pattern condition. The simulation time was extended from 15 to 20 minutes in order to give the filters more time to converge.

The analysis method has been the same that was described at the beginning of subsection 3.4. The total number of simulations was 275. The results are summarised in figures 10, 11 and 12.

In comparison with the isotropic case, Figure 10 presents a significant degradation in the performance of all the filters. The RMSE is increased up to two orders of magnitude.

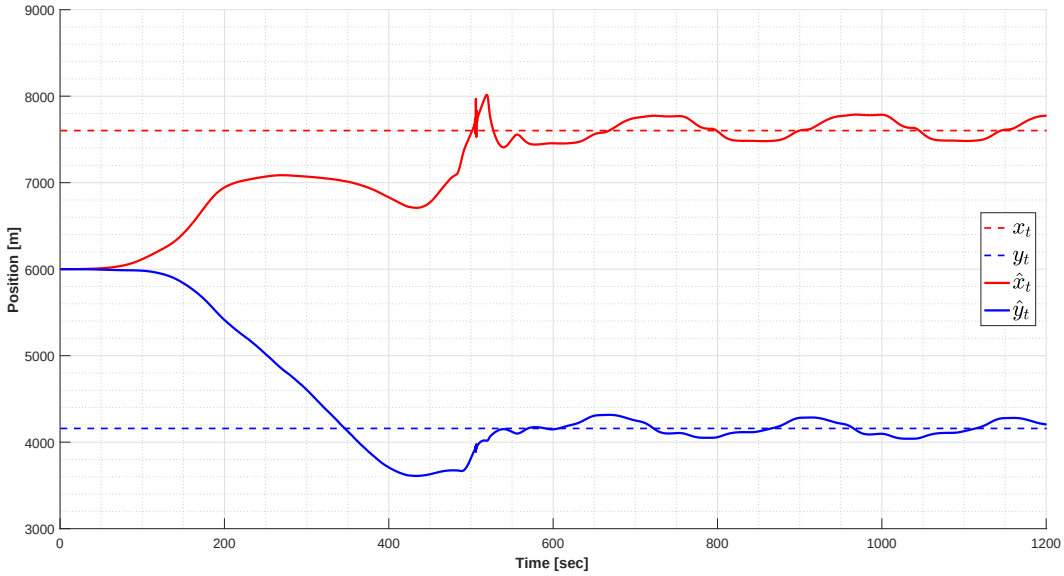

Figure 9: EKF performance example under anisotropic conditions

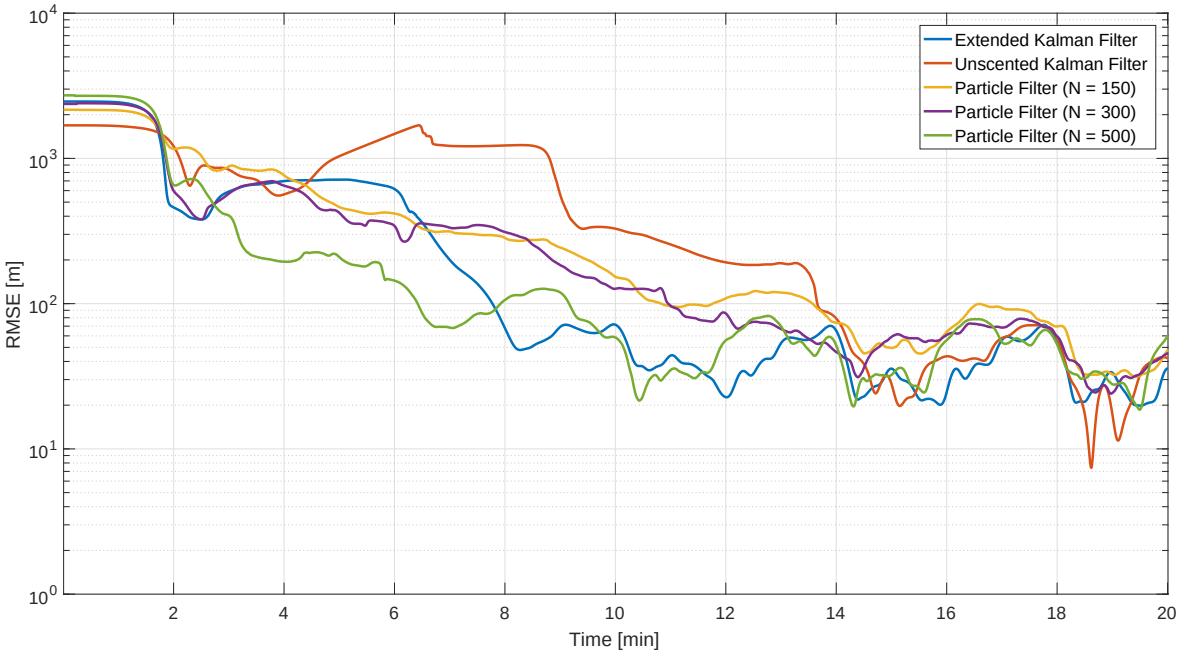

Figure 10: RMSE evolution. Anisotropic case. Original filters

The RMSE evolution is very similar for the 5 filters, especially in the last minutes, when all the filters converge to an error between 30 and 60 m. In general, all the filters manage to gradually diminish the error up to a point, around minute 15, when they get stuck and unable to continue reducing it.

Taking a look to the final estimation error distribution, Figure 11 demonstrates that all the three PFs achieve a much greater percentage of final estimations with an error

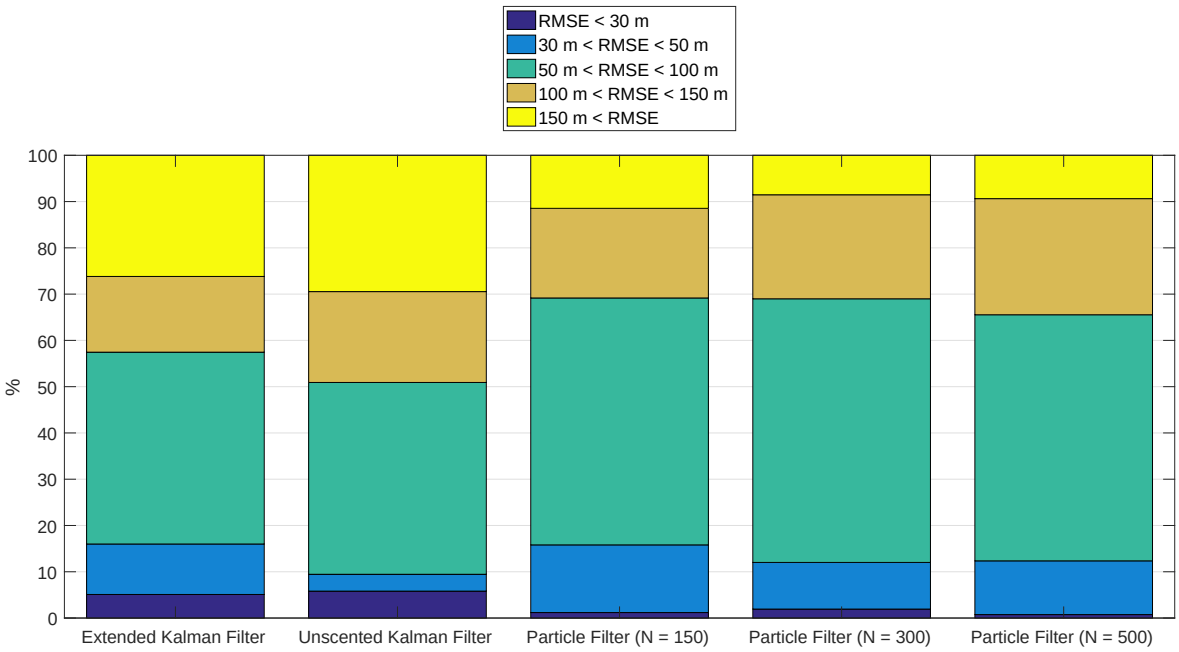

Figure 11: Final Estimation Error Distribution. Anisotropic case. Original Filters

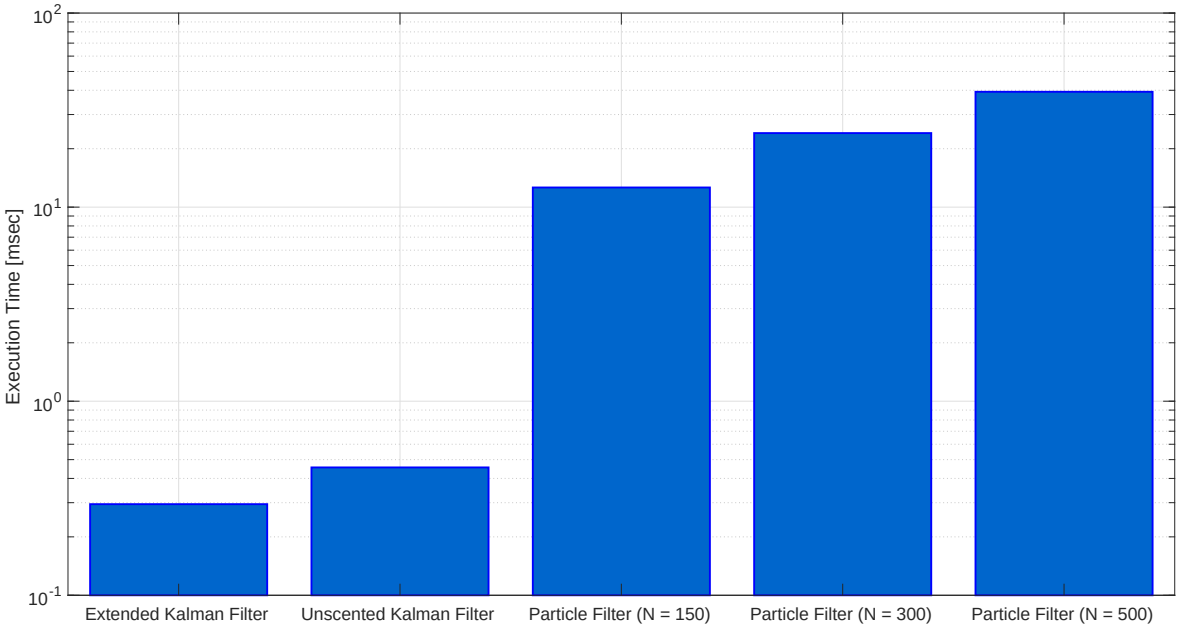

Figure 12: Mean Filter Execution Time. Anisotropic case. Original filters

below 100 m. However, the chances of getting an error below 50 m are low, around 10 % all the filters.

However, the relatively better performance of the PF comes at a cost. Figure 12 shows that PF run times are up to two order of magnitude longer than EKF and UKF. Such long execution times can even make unfeasible to run the estimator on-line.

We can conclude that, despite the significant increment in run time, the PF is slightly more robust against the uncertainty brought by the variable transmitter gains ratio.

Several modifications to the original algorithms have been tested. In the following subsections, those that show to be more promising are presented.

4.2 EKF with smoothing

Taking a look to the evolution of the estimation at the last stages of the simulation, it can be noticed that it shows an oscillatory behaviour around the real state once the UAV goes into the orbit (Figure 9).

For this reason, the first proposed modification consists on performing an smoothing of the estimated state once the UAV enters the orbit.

The main body is the same as EKF. A smoothing parameter β is defined together with a point from which the smoothing starts to be made, k_smooth and the number of past states that are taken into account, N_s. Once the step k is greater, the state estimation returned by the EKF is smoothed according to equation (26).

$$\underline{\hat{x}}_k = \beta \underline{\hat{x}}_k + (1-\beta)\,\frac{1}{N_s} \sum_{i=k-N_s}^{k-1} \underline{\hat{x}}_i \tag{26}$$

After several tests, $\beta = 0.7$ and $N_s = 450$ were the parameters value that provide the best results. The process and measurement noise covariance matrices remain the same.

4.3 Augmented UKF and EKF

As it is not possible to have a priori knowledge about the jammer radiation pattern, the second proposed modification consists on augmenting the state vector including the transmitter gains ratio

$$\underline{x}_k = \begin{bmatrix} x_k \\ y_k \\ G_{t,k}/G_{t,1} \end{bmatrix}$$

This can be easily implemented in the original EKF code. The only relevant change that has to be made is the modification of the Jacobian matrix.

We know that $G_{t,k}/G_{t,1}$ varies with relative elevation and azimuth of the UAV with respect to the jammer and, as a result, $G_{t,k}/G_{t,1}$ is a function of x_k nor y_k. However, it is not possible to know this relationship. For the sake of simplicity, we assumed that $G_{t,k}/G_{t,1}$ is not dependent on x_k nor y_k, so $\frac{\partial G_{t,k}/G_{t,1}}{\partial x_k}$ and $\frac{\partial G_{t,k}/G_{t,1}}{\partial y_k}$ are identically null.

As a result, the Jacobian matrix of the measurement equation (6) is given by equation (27), where $i = 1$.

$$H_{k,i}^{T}(\underline{x}_k) = \begin{bmatrix} 2\frac{G_{t,k}}{G_{t,i}}\left(\frac{x_k - x_{s,i}}{\left(x_k - x_{s,k}\right)^2 + \left(y_k - y_{s,k}\right)^2 + {h_0}^2} - \frac{\left((x_k - x_{s,i})^2 + (y_k - y_{s,i})^2 + {h_0}^2\right)\left(x_k - x_{s,k}\right)}{\left(\left(x_k - x_{s,k}\right)^2 + \left(y_k - y_{s,k}\right)^2 + {h_0}^2\right)^2}\right) \\ 2\frac{G_{t,k}}{G_{t,i}}\left(\frac{y_k - y_{s,i}}{\left(x_k - x_{s,k}\right)^2 + \left(y_k - y_{s,k}\right)^2 + {h_0}^2} - \frac{\left((x_k - x_{s,i})^2 + (y_k - y_{s,i})^2 + {h_0}^2\right)\left(y_k - y_{s,k}\right)}{\left(\left(x_k - x_{s,k}\right)^2 + \left(y_k - y_{s,k}\right)^2 + {h_0}^2\right)^2}\right) \\ \frac{(x_t - x_{s,i})^2 + (y_t - y_{s,i})^2 + h_0^2}{(x_t - x_{s,k})^2 + (y_t - y_{s,k})^2 + h_0^2} \end{bmatrix} \tag{27}$$

No relevant changes are needed in the UKF.

Another static dynamic model is assumed for the evolution of the gains ratio so F matrix becomes the identity matrix of order 3. The process covariance matrix also needs to be changed to take into account the new state.

$$F = \begin{bmatrix} 1 & 0 & 0 \\ 0 & 1 & 0 \\ 0 & 0 & 1 \end{bmatrix}, Q = \begin{bmatrix} 2 & 0 & 0 \\ 0 & 2 & 0 \\ 0 & 0 & 0.005 \end{bmatrix}$$

As we are estimating the transmitter gains ratio, the uncertainty on the measurement is assumed to be reduced, $R = [0.8^2]$.

Figure 13 depicts the results from a simulation in which the transmitter gains ratio were estimated. The estimation is quite bad at the beginning but after a while, it becomes quite good.

4.3.1 EKF with changing reference step

Until now, the reference step, this is the step with respect to which the received power is compared, has remained unchanged. Instead of using the received power ratio with respect to the first step, using the ratio with respect to a few steps behind the current state may, in theory, help to keep the gains ratio almost constant an equal to the unity.

The original code provided with this assignment always calculates the received power ratio with respect the first step. However, it is trivial implement the modification of the reference from step 1 to step i following equation (28).

$$\alpha_{k,i} = \frac{P_{r,k}}{P_{r,i}} = \frac{P_{r,k}/P_{r,i}}{P_{r,i}/P_{r,1}} = \frac{\alpha_{k,1}}{\alpha_{i,1}} \tag{28}$$

Setting the reference 5 steps behind the current iteration provided satisfactory results.

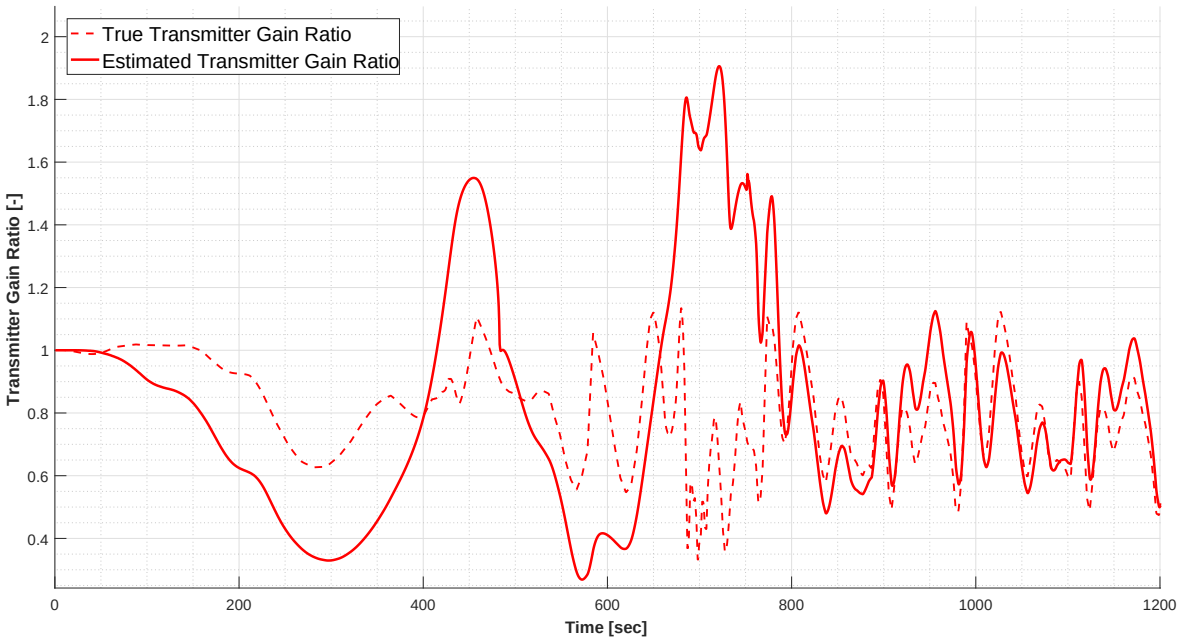

Figure 13: Example of Transmitter gain estimation with augmented EKF

4.4 Alternative Filters Performance

Given good results obtained with the EKF in the isotropic case and mainly because of its short execution time, the proposed alternatives have been implemented and analysed within an EKF structure.

The analysis methodology has been identical to those of the previous estimators. The performance of all the proposed alternative filters is compared to that of the original one in the following charts.

Regarding Figure 14, the most outstanding characteristic may be the unexpected low performance of the EKF with state augmentation, which is significantly worse than the rest of filters. The reader may notice as well that, apparently, none of the other alternatives achieves a dramatic improvement of the accuracy. However, the two last alternatives, do manage to decrease the error.

In fact, if we take look to Figure 15, it is possible to check the significant improvements achieved by the two former proposed filters. 40% of the time, the smoothing strategy manages to predict the jammer position with an error less than 30 m. On the other hand, EKF with changing reference locates the jammer with an accuracy under 100 m about 95% of the time.

Finally, it is worth mentioning that the significant improvement on the accuracy and frequency of accurate estimations is brought at a minor cost in computational time, as it is shown in Figure 16. This last figure also shows that the augmented EKF is not only the worst estimator, but also the slowest one.

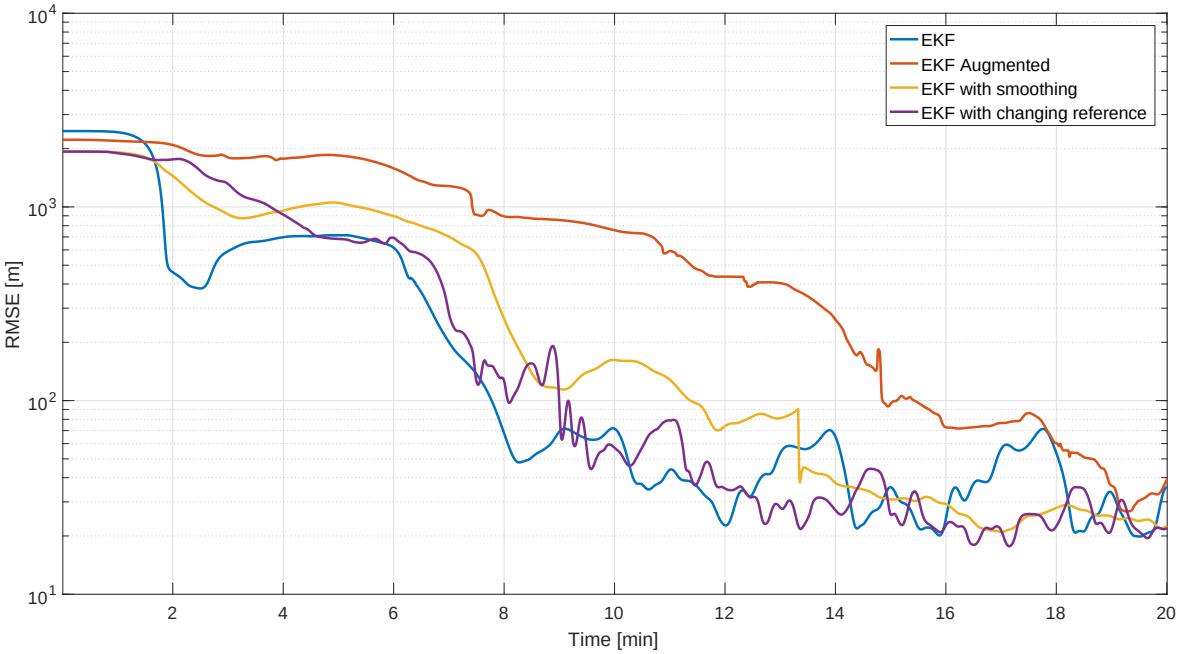

Figure 14: RMSE evolution. Anisotropic case. Alternative Filters

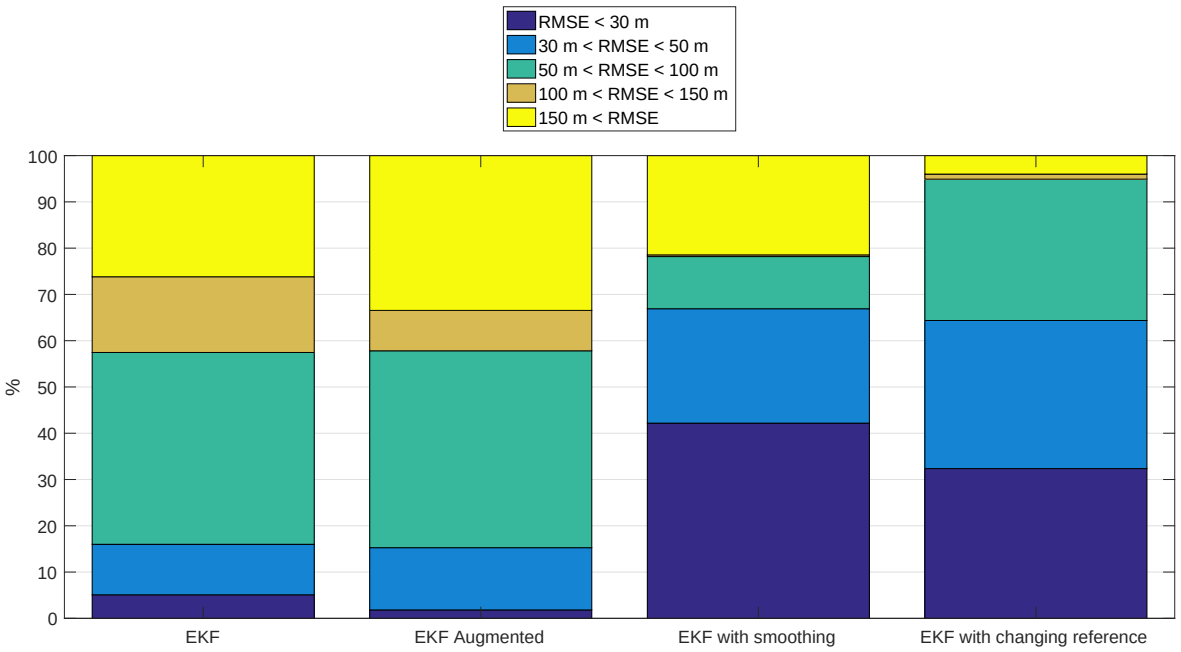

Figure 15: Final Estimation Error Distribution. Anisotropic case. Alternative Filters

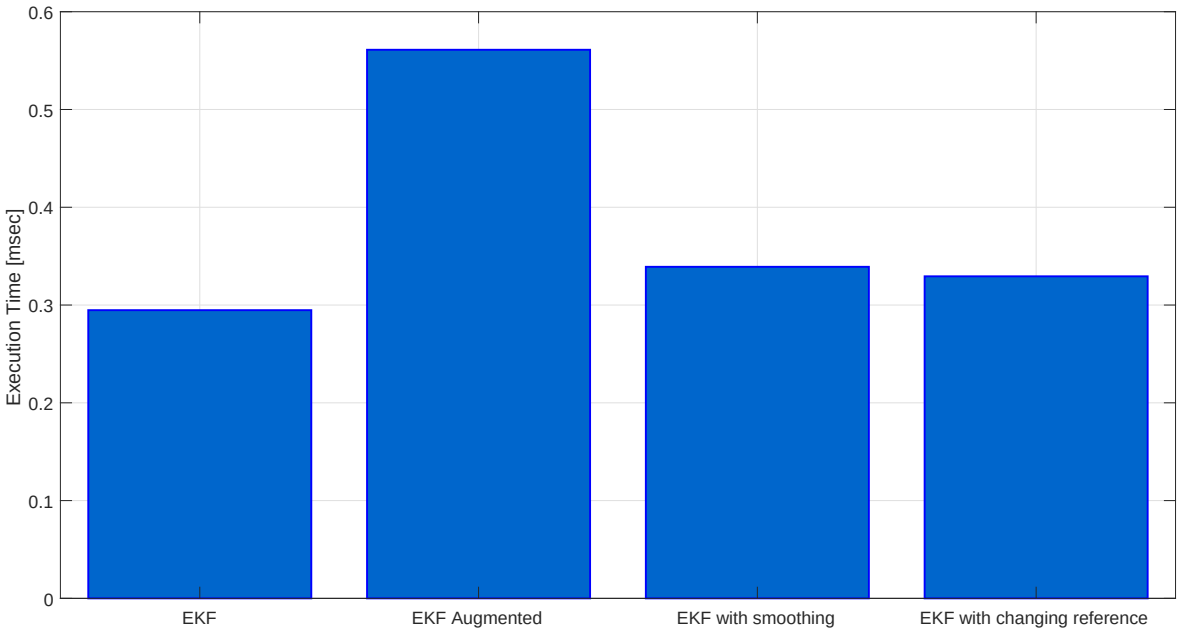

Figure 16: Mean Filter Execution Time. Anisotropic case. Alternative Filters

5 Conclusions

The following concluding remarks are presented as the most important points of this report:

- EKF has demonstrated an outstanding performance. Particularly, if the situation allows to assume an isotropic radiation pattern, EKF is, without doubt, the most advisable solution to the estimation problem.
- UKF has presented a performance very similar to the EKF with a slightly increment in the run time. However, a finer parameter adjustment may improve its performance.
- The great increment on execution time together with the degradation of the estimation accuracy have proved that PF is the less efficient state estimator for this particular application.
- The anisotropic radiation pattern has shown to be a real challenge to all the three unmodified filters. In this case, contrary to the last point, the PF demonstrated to be more robust against the uncertainty in the transmitter gains ratio. The PFs were the estimators that provided the most accurate results. However, they were not good enough.
- Two of the proposed modifications demonstrated to be a success, with accuracies under 30 metres. These alternatives were the smoothing of the EKF estimation (subsection 4.2) and the continuous change of the reference step (subsection 4.3.1).
- Achieving the same level of accuracy in the anisotropic case is not possible with none of the proposed alternatives. Further testing and tuning of the parameters may help to improve the results. However, given that the radius of the orbit is 1 km, the jammer is ensured to be within the UAV orbit. Other sensors, such an on board camera, could be used then to try to obtain a more accurate position estimation.
- In order to try to improve the accuracy, implementing and testing other estimation strategies (e.g. fixed-interval smoother, iterative filters) is highly advisable.

This page intentionally left blank.

References

[1] E. W. Frew, D. A. Lawrence, and S. Morris, "Coordinated standoff tracking of moving targets using Lyapunov guidance vector fields," *Journal of guidance, control, and dynamics*, vol. 31, no. 2, pp. 290–306, 2008.

[2] S. J. Julier and J. K. Uhlmann, "New extension of the Kalman filter to nonlinear systems," in *AeroSense'97*. International Society for Optics and Photonics, 1997, pp. 182–193.

[3] Y. Cao. (2008) Learning the Unscented Kalman Filter. [Online]. Available: https://uk.mathworks.com/matlabcentral/fileexchange/18217-learning-the-unscented-kalman-filter

[4] S. J. Julier and J. K. Uhlmann, "Unscented filtering and nonlinear estimation," *Proceedings of the IEEE*, vol. 92, no. 3, pp. 401–422, 2004.

[5] M. S. Arulampalam, S. Maskell, N. Gordon, and T. Clapp, "A tutorial on particle filters for online nonlinear/non-gaussian bayesian tracking," *IEEE Transactions on signal processing*, vol. 50, no. 2, pp. 174–188, 2002.

[6] D. A. A. Marn. (2012) Particle filter tutorial. [Online]. Available: https://es.mathworks.com/matlabcentral/fileexchange/35468-particle-filter-tutorial